8-5-2014

Compact Verilog-A Modeling of Silicon Traveling-Wave Modulator for Hybrid CMOS Photonic Circuit Design

Kehan Zhu
Boise State University

Vishal Saxena
Boise State University

Wan Kuang
Boise State University

 doi: 10.1109/MWSCAS.2014.6908490

Compact Verilog-A Modeling of Silicon Traveling-Wave Modulator for Hybrid CMOS Photonic Circuit Design

Kehan Zhu, Vishal Saxena, Wan Kuang
Department of Electrical and Computer Engineering, Boise State University, Boise, ID 83725.
Email: kehanzhu@u.boisestate.edu

***Abstract*—A compact Verilog-A model of silicon-based junction traveling-wave Mach-Zehnder modulator (MZM) is developed for hybrid CMOS and photonic system-level simulation in Cadence environment. Critical device functions such as the voltage dependent change of refractive index, small-signal RLGC parameters for the MZM arms are extracted from the photonic device characterization from OpSIS foundry. Thermo-optical coefficient is also considered in the model. Simulation results including electro-optic S21 is characterized for the phase modulator's bandwidth. Also, transient MZM operation with non-return to zero (NRZ) data transmission at 10 Gb/s and 20 Gb/s rates are demonstrated.**

***Index Terms*—CMOS Photonics, Compact model, MZM, NRZ, Verilog-A.**

I. Introduction

SILICON photonic platforms are emerging as important enablers for high-speed data communication, as they combine the large instantaneous bandwidth of the photonic devices with signal processing abilities of CMOS electronics [1]. The CMOS photonic paradigm also opens several opportunities for the integrated circuit (IC) designers to adopt new techniques from the photonic community and gainfully combine them with conventional electronics to realize novel system-level functionality. Further, designing CMOS circuits to interface with silicon photonic devices requires high level of optoelectronic integration. In the past, silicon photonic devices were typically made by designers trained in optics, with specialized device simulators and field solvers, that are not at all compatible with the traditional IC design flow. There are commercially available tools for photonic device and circuit simulation such as Lumerical computational solutions [2]. Recent progress has been made with optical system-level design tools such as the Lumerical's Interconnect [2]. However, such tools are specific to photonic integrated circuits (PIC) simulation and cannot be employed for hybrid optoelectronic system simulation, where a SPICE-like solver is required for transistor-level circuit simulations. Thus, IC designers that design circuits for integration with silicon photonics, need compact photonic device models which encapsulate both electrical as well as optical properties for the Electrical-Optical (EO) hybrid circuit simulation. Verilog-A, a hardware description language developed for behavioral modeling of analog circuits, is a good candidate for addressing this essential need [3]. There has been a general lack of such compact models for integrating silicon photonic devices with CMOS electronics, and this work aims to fill the gap by systematically modeling a MZM device using Verilog-A.

This paper presents a convenient and systematic design methodology for modeling silicon traveling-wave MZM with Verilog-A in Cadence environment. Section II explains the working mechanism of the device. Section III describes the compact modeling methodology with Verilog-A. Section IV presents the simulated results from the developed model, suitable for pre-silicon validation. Section V concludes the paper.

II. MZM Device Mechanism

A top view illustration of the MZM fabricated by OpSIS/IME with a cross-section view of the lateral pn junction arm is shown in Fig.1 [4]. The waveguide core consists of lightly doped pn junction, intermediate density p^+ and n^+ regions for reducing series resistance without inducing excessive optical loss, and heavily doped p^{++} and n^{++} implant for contact [4], [5]. The working mechanism of the MZM is described next. The DC light source at 1550 nm is split evenly into two arms of the MZM, an electrical field caused by reverse-biased voltage applied on each of the pn junction arms causes a change in the carrier density, which, in turn induces a phase shift in the optical wave propagating in the MZM arm. When combining the two paths of light together, they interfere either constructively or destructively as seen at the output depending on the E-field selectively applied across their arms. The electro-optic effect used to modulate optical phase in such a device is based on free carrier dispersion mechanism, which can achieve higher modulation speed than the forward-bias carrier injection mechanism [4].

When the signal frequency is very high and the propagation delay of the signal in the arm is significant, the signal should be treated as guided electromagnetic wave. Hence, transmission line effects must be considered in such designs, which will be further discussed later.

Let's assume the input optical source with intensity of I_0 is evenly split into two, where one is traveling an extra length of waveguide causes a phase bias (ϕ_{DC}) between the two arms before reaching the phase modulator [4]. Usually ϕ_{DC} has certain variation that must be tuned by changing the wavelength of the tunable laser or by using a thermal tuning method.

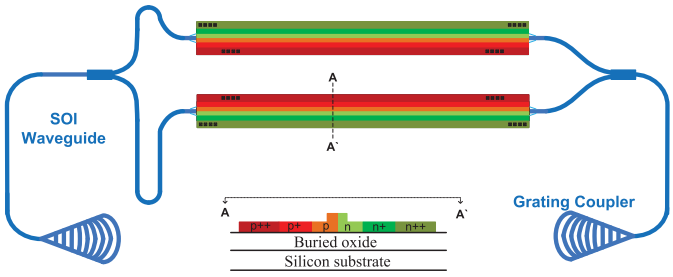

Figure 1. Illustration of the traveling-wave MZM.

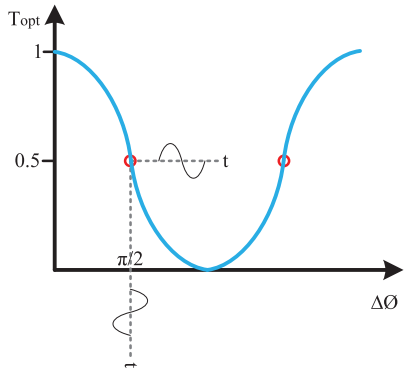

Figure 2. Characteristic optical power transmission function with phase difference of a traveling-wave MZM.

The phase shift, ϕ_{top} and ϕ_{bot}, for the top arm and bottom arm, are a function of the applied voltages, respectively. The output intensity I_{out} is combined as Eq.1.

$$I_{out} = \frac{I_0 e^{j(\phi_{DC}+\phi_0+\triangle\phi_{top})}}{2} + \frac{I_0 e^{j(\phi_0+\triangle\phi_{bot})}}{2} \quad (1)$$

where, ϕ_0 is the phase introduced by in both of the arms and expressed as $(2\pi/\lambda)n_{eff}(V)L$. Further, $n_{eff}(V)$ is the voltage dependent effective refractive index of the waveguide core. The optical power transfer function (T_{opt}) of the MZM can be derived in Eq.2.

$$T_{opt} = \left|\frac{I_{out}}{I_0}\right|^2 = \frac{1+cos\left(\phi_{DC}+\triangle\phi_{top}-\triangle\phi_{bot}\right)}{2} \quad (2)$$

We define $\Delta\phi = \phi_{DC} + \triangle\phi_{top} - \triangle\phi_{bot}$ as the absolute phase difference between the two arms, where ϕ_{DC} can be externally set to the quadrature bias point ($\pi/2$) in the developed compact model to achieve the best linearity of modulation as shown in Fig.2. While the small-signal phase shift induced in the top arm and bottom arm, $\triangle\phi_{top}$ and $\triangle\phi_{bot}$, of the MZM is caused by the change of refractive index modulated by the applied voltage (V), are defined as Eq.3. The MZM modulation figure of merit, $V_\pi L_\pi$, is defined as the phase shift ($\Delta\phi_{dut}$) due to the applied voltage ($V_{applied}$) on the length (L_{dut}) of the arm, can be expressed as $V_\pi L_\pi = \frac{\pi}{\Delta\phi_{dut}} V_{applied} L_{dut}$ [5]. For the lower voltage operation, longer MZM arms are desired. However, longer the arm, the more optical loss will be introduced.

$$\triangle\phi_{top,bot} = \frac{2\pi}{\lambda}\cdot\Delta n_{eff}(V)\cdot L \quad (3)$$

III. MZM Verilog-A Model Partition

The traveling-wave MZM model shown in Fig.3 is partitioned into three sub-blocks: power splitter, distributed phase modulator and combiner. A 3-mm length for each of the arms is used in the model. In order to display the units for optical power (OptPower) and optical phase (OptPhase) in the unit of Watts and radians, respectively, their natures should be added explicitly as a Verilog-A discipline [6]. Since Verilog-A doesn't support complex numbers, the power intensity and phase are processed separately in each of the MZM arms. Finally, these quantities are combined in the combiner block. At the core of the model lies the phase modulator module, which is detailed later in section III B.

A. Power Splitter

The power splitter is the first block in the MZM, which evenly splits the source. Different propagation delay and loss scale (Eq.4) can be introduced by a longer length for one waveguide than the other, as mandated by the phase bias. The phase bias is not added in the splitter model but added externally to the phase modulator. In Eq.4, c and α is the speed of light and loss factor (dB per length), respectively. c/n_{eff} is the wave velocity and a 0.3 dB/mm loss factor is used here for this undoped waveguide medium. By using Verilog-A absolute delay operator, the output power (Out) can be expressed with respect to the input source (In) with a split coefficient (k=0.5) as $OptPower(Out)$ <+ $absdelay(OptPower(In)*loss*k, prog\_delay)$;.

$$prog\_delay = \frac{L\cdot n_{eff}}{c} \;\; and \;\; loss = 10^{-\alpha\cdot L} \quad (4)$$

B. Distributed Phase Modulator

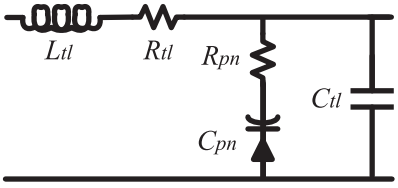

Figure 4. Schematic of the distributed RLGC network of the MZM arm.

Each of the MZM arms is modeled using two sub-modules. One is the distributed RLGC network for the electrical component of the path as shown in Fig.4. Another sub-module concerns with the optical phase modulation related to Fig.5. In Fig.4, R_{tl} is a frequency-dependent metal skin resistance, which changes from 2.5 Ω/mm at very low frequencies up to 10 Ω/mm at 40 GHz. However, it is kept as a constant (e.g. 5 Ω/mm at 10 GHz) in the model for simplicity and without losing accuracy at the same time. Moreover, the value shown in the component description format (CDF) parameter can be overwritten for other frequencies by editing the object properties of the symbol in Cadence. L_{tl} and C_{tl} are the inductance and capacitance between the metal traces, respectively, which are also frequency-dependent [5]. The

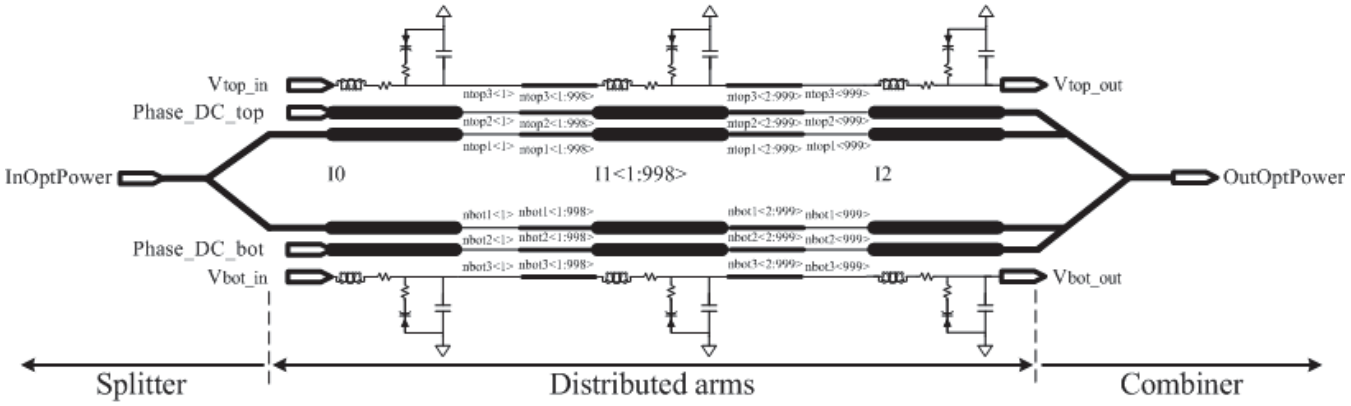

Figure 3. Schematic illustration of the developed Verilog-A MZM model.

transconductance (G) consists parasitic resistance (R_{pn}) and capacitance (C_{pn}) from the electrodes to the edges of the pn junction depletion region is explicitly included in the model. The C_{pn} is primarily contributed by the depletion capacitor of the pn junction, which varies with applied reverse-bias voltage as shown in Fig.5 [4]. The RLGC parameters used for the modeling at 10 GHz are listed in Table 1. For the distributed elements which are concatenated to form the MZM arm, the output phase of each of the stages reflects the voltage-dependent phase-change induced by the current stage, added to the phase from the previous stage. Voltage dependent refractive index change derived from [4] is also plotted in Fig.5. By using Eq.3 we can calculate the phase change along each of the arms. Functions for the C_{pn} and Δn_{eff} curves plotted in Fig.5 are extracted using a 4^{th}-order polynomial curve-fit, shown in Eq.5 and Eq.6, respectively, which are incorporated in the Verilog-A code. However, it should be noted that the valid voltage range for the model is limited to -0.3-4 V. The change of phase in one segment ($\triangle\phi_{seg}$) considering thermo-optic coefficient of the refractive index (dn/dT), which is about 1.86 $\times 10^{-4}/°$C [7], is included in Eq.7. A fitting coefficient of 0.9 for the effective refractive index is used in the model. As shown in Fig. 3, both arms consist of one thousand distributed RLGC elements. The output phase ($PhaseOut$) with respect to the input phase ($PhaseIn$) expressed in Verilog-A absolute delay operator as: $OptPhase(PhaseOut)$ <+ $absdelay(OptPhase(PhaseIn)$ + $delta\_phase, prog\_delay)$;. Here, the parameter $delta\_phase$ corresponds to $\triangle\phi_{seg}$. The optical power relation is the same as discussed above, except that the loss factor (α) is 0.63 dB/mm is introduced for the doped waveguide.

$$C_{pn} = 0.0023V^4 - 0.02V^3 + 0.06V^2 - 0.09V + 0.23\ (fF/\mu m) \quad (5)$$

$$\Delta n_{eff} = -6\times10^{-7}V^4 + 6.8\times10^{-6}V^3 - 3\times10^{-5}V^2 + 10^{-4}V - 6\times10^{-6} \quad (6)$$

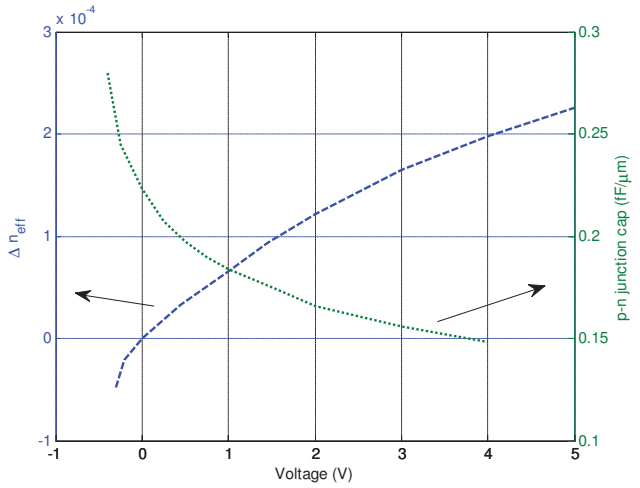

Figure 5. The change of refractive index and pn junction capacitance as a function of the voltage.

$$\triangle\phi_{seg} = \frac{2\pi}{\lambda}[0.9\cdot\Delta n_{eff} + \frac{dn}{dT}(T - T_0)]\cdot L \quad (7)$$

Table 1. RLGC parameters at 10 GHz.

R_{tl}	L_{tl}	R_{pn}	C_{tl}
5 Ω/mm	450 pH/mm	15 $\Omega\cdot mm$	123 fF/mm

C. Combiner

The combiner block finally merges the optical power from the two arms and is multiplied by the power transfer function. The power transfer function is a function of the phase difference between the two arms described in Eq.2. As shown in Fig.3, the phase difference can also also be probed for verification during the simulation.

IV. Simulation Results

The electro-optic (EO) S21 of one arm is characterized by performing S-parameter analysis in Cadence Spectre with the RLGC parameters listed in Table 1, and is shown in Fig.6. With a termination of 50 Ω, the -3 dB bandwidth is 13 GHz

and 16 GHz, respectively, when is reverse-biased at 0 V and 1 V. From the EO S21 bandwidth, it can be predicted that the bandwidth of the modeled MZM configuration is about 15 GHz, which indicates that it can be best operating below 12.5 Gb/s (without equalization), if the system bandwidth requirement is set to 1.2 times higher than the data rate. However, it should be noted that the RLGC parameters used here is best suited at 10 GHz bandwidth. The developed model is used to demonstrate an NRZ data transmission. With a 1 mW optical source, modulated by a data rate of 10 Gb/s and 20 Gb/s $2^{31}-1$ PRBS electrical voltage with an amplitude of 1.2 V, respectively. The eye diagrams of the optical output for both cases are plotted in Fig.7, which shows very good eye opening at 10 Gb/s. The eye diagram further reveals that the modulator exhibits more bandwidth limited inter-symbol interference (ISI), and the amplitude is also decreased, as the data rate goes up to 20 Gb/s. The simulated peak-to-peak jitter is about 0.66 ps and 3.87 ps for 10 Gb/s and 20 Gb/s data-rates, respectively. It achieves an extinction ratio (ER) of 10.2 dB and 9.6 dB for the each case, respectively.

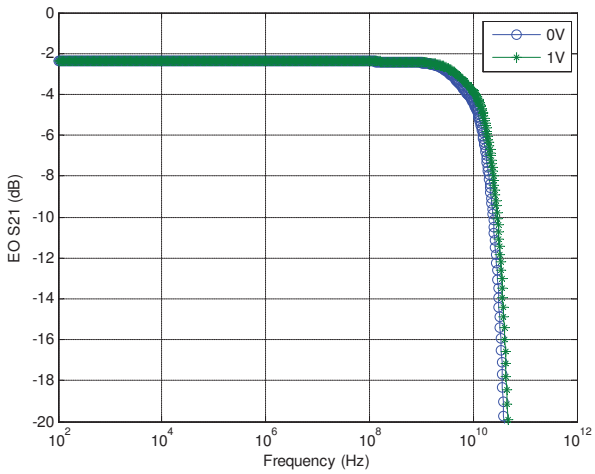

Figure 6. EO S21 of a 3-mm phase modulator reverse biased at 0 V and 1 V.

V. Conclusion

This work presents a Verilog-A model which can capture the electrical and optical characteristics of a traveling-wave MZM realized on a silicon photonic platform. With this compact model, hybrid circuit simulation with CMOS transistors and photonic devices becomes possible. Simulation results including EO S21 is characterized for modulator bandwidth and eye diagrams for data rate at 10 Gb/s and 20 Gb/s $2^{31}-1$ PRBS NRZ data are demonstrated. Moreover, performance parameters for a modulator such as the peak-to-peak jitter and ER have been demonstrated . The proposed design and simulation methodology is to be used for complex system and circuit level simulations and can be extended to other photonic devices. The simulated results for the design will be compared with experimental results obtained from prototype chips in future publications.

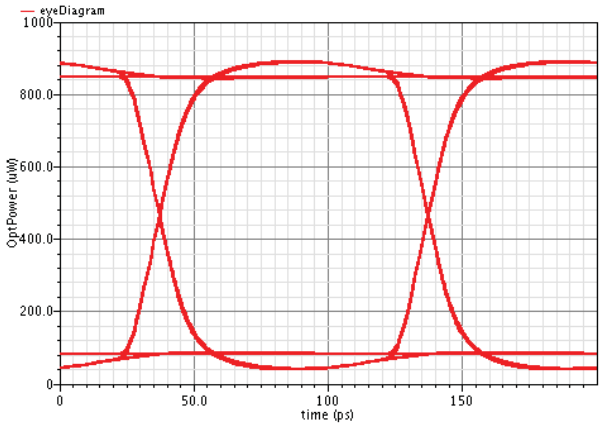

(a) 10 Gb/s

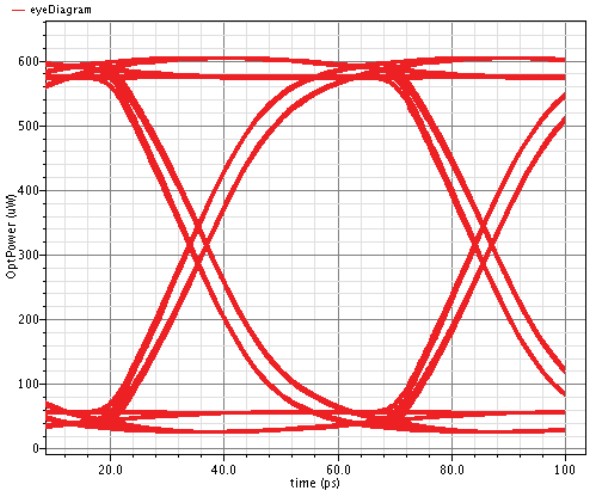

(b) 20 Gb/s

Figure 7. Simulated optical output eye diagrams of the MZM at (a) data rate of 10 Gb/s, (b) data rate of 20 Gb/s $2^{31}-1$ PRBS data.

Acknowledgment

The authors gratefully acknowledge the OpSIS service for facilitating silicon photonic IC design and fabrication, and thorough discussions with Ran Ding and Zhe Xuan from University of Delaware during the compact model development. Partial support from NASA ISGC is acknowledged.

References

[1] M. Hochberg, N. C. Harris, R. Ding *et al.*, "Silicon photonics: the next fabless semiconductor industry," *IEEE Solid-State Circuits Magazine*, vol. 5, no. 1, pp. 48–58, 2013.

[2] Lumerical Solutions, Inc. https://www.lumerical.com/. [Online]. Available: https://www.lumerical.com/

[3] S. Fathpour and B. Jalali, *Silicon photonics for telecommunications and biomedicine*. CRC Press, 2011.

[4] T. Baehr-Jones, R. Ding, Y. Liu *et al.*, "Ultralow drive voltage silicon traveling-wave modulator," *Opt. Exp.*, vol. 20, no. 11, pp. 12 014–12 020, May 2012.

[5] R. Ding, Y. Liu, Q. Li *et al.*, "Design and characterization of a 30-GHz bandwidth low-power silicon traveling-wave modulator," *Opt. Commun.*, vol. 321, pp. 124–133, 2014.

[6] K. Kundert and O. Zinke, *The designer's guide to Verilog-AMS*. Springer, 2004.

[7] P. Dong, W. Qian, H. Liang *et al.*, "Low power and compact reconfigurable multiplexing devices based on silicon microring resonators," *Opt. Exp.*, vol. 18, no. 10, pp. 9852–9858, May 2010.